J Fluoresc (2012) 22:737–744
DOI 10.1007/s10895-011-1009-x

ORIGINAL PAPER

# Kamlet-Taft and Catalan Studies of Some Novel Y-Shaped Imidazole Derivatives

**J. Jayabharathi · V. Thanikachalam · K. Brindha Devi · M. Venkatesh Perumal**

Received: 28 May 2011 / Accepted: 20 October 2011 / Published online: 9 November 2011


**Abstract** Some novel Y-shaped imidazole derivatives were developed and characterized by NMR and mass spectral techniques. The photophysical properties of these imidazole derivatives were studied in several solvents. The Kamlet-Taft and Catalan's solvent scales were found to be the most suitable for describing the solvatochromic shifts of the absorption and fluorescence emission. The adjusted coefficient representing the electron releasing ability or basicity of the solvent, $C_\beta$ or $C_{SB}$ has a negative value, suggesting that the absorption and fluorescence bands shift to lower energies with the increasing electron-donating ability of the solvent. This effect can be interpreted in terms of the stabilization of the resonance structures of the chromophore. The observed lower fluorescence quantum yield may be due to an increase in the non-radiative deactivation rate constant. This is attributed to the loss of planarity in the excited state provided by the non co-planarity of the cinnamaldehyde ring attached to C(2) atom of the imidazole ring. Such a geometrical change in the excited state leads to an important Stokes shift, reducing the reabsorption and reemission effects in the detected emission in highly concentrated solutions.

**Keywords** NMR · Kamlet-Taft · Catalan parameters · Aggregation

J. Jayabharathi (✉) · V. Thanikachalam · K. B. Devi · M. V. Perumal
Department of Chemistry, Annamalai University, Annamalainagar,
608 002, Tamilnadu, India
e-mail: jtchalam2005@yahoo.co.in

## Introduction

Recently, heterocyclic imidazole derivatives have attracted considerable attention because of their unique optical properties [1]. These compounds play very important role in chemistry as mediators for synthetic reactions, primarily for preparing functionalized materials [2]. Imidazole nucleus forms the main structure of some well-known components of human organisms and also has significant analytical applications such as laser [3], polymer stabilizer [4], Raman filters [5] environmental probes in biomolecules [6], etc. by utilizing their fluorescence and chemiluminescence properties.

Several factors contribute to the best laser performance of pyrromethene with respect to rhodamine as laser dye [7]: (1) low triplet-triplet absorption capacity at the lasing spectral region, which reduces the losses in the resonator cavity; (2) a poor tendency to self-aggregate in organic solvents, avoiding the fluorescence quenching of the monomer emission by the presence of aggregates in highly concentrated solutions, as was observed in rhodamine dyes: (3) and their high photostability [8, 9], which improves the lifetime of the laser action with respect to that of rhodamines [10]. Owing to these properties, PM dyes have been successfully incorporated into different solid matrixes (polymers, silica, etc.,) [11] to develop solid-state syntonizable dye lasers.

Photophysical properties and laser characteristics of compounds in liquid solutions and in polymeric matrixes [11], indicating that the laser behaviour is a consequence of the photophysical properties. Indeed, the evolution of the fluorescence wavelength and quantum yield with several environmental factors was similar to that observed for the laser band and efficiency, respectively. The Stokes shift modifies the lasing performance [12] in highly concentrated

solutions because it affects the reabsorption and reemission phenomena, which shifts the emission band to longer wavelengths and reduces its efficiency [13]. In the present paper, the photophysical properties of imidazole derivatives 1 and 2 were investigated in a wide variety of solvents, including apolar, polar and protic solvents. The solvent effects on the absorption and fluorescence bands are analyzed by a multi-component linear regression in which several solvent parameters are simultaneously analyzed. The fluorescence quantum yield and the Stokes shift are analyzed to look for the best conditions to improve the lasing efficiencies of these derivatives.

## Experimental

### Materials and Methods

Benzil (Sigma-Aldrich Ltd.), cinnamaldehyde, *p*-hydroxy cinnamaldehyde, *p*-methyl aniline (S.D. fine.) and all the other reagents were used without further purification.

### Optical Measurements and Composition Analysis

NMR spectra were recorded on a Bruker 400 MHz instrument. The ultraviolet–visible (UV–vis) spectra were measured on UV–vis spectrophotometer (Perkin Elmer, Lambda 35) and corrected for background due to solvent absorption. Photoluminescence (PL) spectra were recorded on a (Perkin Elmer LS55) fluorescence spectrometer. MS spectra were recorded on a Varian Saturn 2200 GCMS spectrometer.

### Computational Details

Quantum mechanical calculations were used to carry out the optimized geometry, with Guassian-03 program using the Becke3-Lee-Yang-Parr (B3LYP) functional supplemented with the standard 6–31 G(d,p) basis set [14].

### General Procedure for the Synthesis of Imidazole Derivatives 1–3

The experimental procedure was used as the same as described in our recent papers [15–26]. The imidazole derivatives were synthesized from an unusual four components assembling of benzil, ammonium acetate, aniline and the corresponding aldehydes (Scheme-1).

### 4,5-Diphenyl-2(*E*)-Styryl-1H-Imidazole (1)

Yield: 55%. mp : 260 °C, Anal. calcd. for $C_{23}H_{18}N_2$: C, 85.68; H, 5.63; N, 8.69. Found: C, 84.89; H, 5.23; N, 7.93. $^1$H NMR (500 MHz, $CDCl_3$): δ 9.87 (s, 1H), 8.09 (d, 1H), 8.01 (d, 1H), 7.98–6.79 (m, 15H). $^{13}$C (100 MHz, $CDCl_3$): δ 145.56, 136.48, 133.40–125.49 (Aromatic carbons). MS: m/e 322.15, calcd 321.68.

### 4,5-Diphenyl-2(E)-Styryl-1-*p*-Tolyl-1H-Imidazole (2)

Yield: 55%. mp : 168 °C, Anal. calcd. for $C_{30}H_{24}N_2$: C, 87.35; H, 5.86; N, 6.79. Found: C, 86.57; H, 5.14; N, 7.57. $^1$H NMR (500 MHz, $CDCl_3$): δ 2.33 (s, 3H), 6.84 (d, 2H), 8.01–7.03 (m, 19H). $^{13}$C (100 MHz, $CDCl_3$): δ 24.1, 110.16, 122.4, 127.45–135.89 (Aromatic carbons). MS: m/e 412.19, calcd 410.57.

### 4-((E)-2-(4,5-Diphenyl-1-*p*-Tolyl-1H-Imidazol-2-yl)vinyl) phenol (3)

Yield: 55%. mp : 165 °C, Anal. calcd. for $C_{30}H_{24}N_2O$: C, 84.08; H, 5.65; N, 6.54. Found: C, 83.13; H, 5.02; N, 7.33. $^1$H NMR (500 MHz, $CDCl_3$): ): δ 2.31 (s, 3H), 5.31 (s, 1H), 6.89 (d, 2H), 8.05–6.98 (m, 18H). $^{13}$C (100 MHz, $CDCl_3$): δ 24.1, 110.16, 122.4, 127.45–135.89 (Aromatic carbons). MS: m/e 428.19, calcd 426.97.

## Results and Discussion

### Steric Hindrance in Imidazoles: X-Ray Analysis

DFT calculation of Y-shaped imidazole derivatives reveal that the imidazole ring is essentially planar [27] and makes dihedral angle around 166.0° with the cinnamaldehyde ring. Three key twists, designated as $\alpha$, $\beta$ and $\gamma$ have been examined. $\alpha$ is used to indicate the twist of imidazole ring from the aromatic six-membered ring at C(2), $\beta$ and $\gamma$ are used for twists of imidazole ring from phenyls at C(5) and C(4) positions, respectively (Fig. 1a). By comparison of results in Table 1 several additional interesting structural features can be concluded that the $\gamma$ twist is always smaller than the $\beta$ twist. The $\beta$ twist originates from the interaction of substituent at N(1) of the imidazole with the phenyl group at C(5) whereas the $\gamma$ twist is a result of the interaction of the phenyl group at C(4) with the other one at C(5). The $\beta$ twist always increases upon the substitution at N(1) of the imidazole derivatives compared to the parent counterparts and the substitution increases the $\beta$ twist but decreases the $\gamma$ twist (Fig. 1b). The present structural information allows us to further explore the correlation between structural features and fluorescent property. It reveals that $\alpha$ twist is correlated with fluorescent property, the larger $\alpha$ twist; the more drops the fluorescence quantum yield. Such a clear correlation indicates the importance of coplanarity between imidazole and the aromatic ring at C

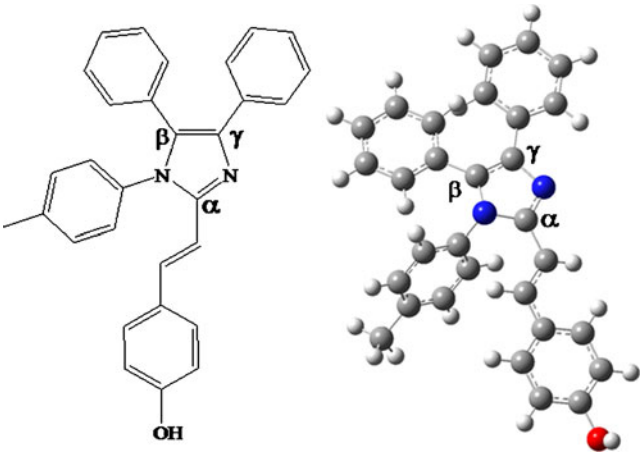


**Fig. 1** (**a**) The key $\alpha$ twist of imidazole ring at C(2) (**b**) Molecular modeling of the imidazole derivative (3) by DFT/B3LYP/6–31 G(d,p)

(2). This correlation can be ascribed to the conjugation rigidity. When the two adjacent aromatic species are in a coplanar geometry, the *p*-orbitals from the C–C bond connecting the two species will have maximal overlapping and the two rings will have a rigid and delocalized conjugation, as the result, the bond is no longer a pure single bond, as evident from the X-ray data of (1). The present bond distance of C2–C21 is 1.454(4) Å (Table 1) is shorter than the regular single bond distance between two sp2 carbons (1.48 Å) [27], because of delocalization.

## Solvent Effects on the Absorption and Fluorescence Properties

All these imidazole derivatives show solvatochromism (Table 2) i.e., changes in the polarity of the solvents, charge transfer takes place and causing colour changes. The position of the longer wavelength absorption and emission bands in the spectra was determined in several protic and aprotic solvents (Fig. 2). Lippert-Mataga [28] plot was constructed for the normal fluorescence spectrum of imidazole derivatives (1–3) (Fig. 3) using the following equation.

$$\nu_{ss}^{-} = \nu_{ab}^{-} - \nu_{fl}^{-} = const + \left[\frac{2(\mu_e - \mu_g)^2}{hca^3}\right] f(D,n) \qquad (4)$$

**Table 1** Deviation parameters (°) of imidazole from other rings

| Compound | (α) | (β) | (γ) | $\phi_f$ | $\tau_f$ (ns) |
|---|---|---|---|---|---|
| 1 | −43.08 | 8.02 | 166.06 | 0.09 | 1.3 |
| 2 | 43.16 | 7.90 | 178.06 | 0.12 | 1.4 |
| 3 | 41.90 | 5.29 | 179.28 | 0.15 | 1.5 |

where $f(D,n) = (D-1)/(2D+1) - (n^2-1)/(2n^2+1)$, indicates the orientation polarizability and depicts polarity parameter of the solvent [29], $n$ is refractive index, D is dielectric constant, $\mu_e$ and $\mu_g$ are dipole moments of the species in $S_1$ and $S_0$ states, respectively, $h$, Planck's constant; $c$, velocity of light and $a$, Onsagar's cavity radius. Stokes shifts were calculated from $\lambda_{max}^{f}$ rather than 0-0-emission transition. The Lippert-Mataga plot is linear for the non-polar and polar / aprotic solvents with excellent correlation coefficient.

Large stokes shifted fluorescence band suggest that this emission has originated from the species which is not present in the $S_0$ state and large geometrical changes have takes place in the species when excited to $S_1$ state and the large stokes shift may be explained by the presence of intermolecular hydrogen bonding of imidazole nitrogen (N2) with polar solvent molecules leading to the stabilization of solvated isomers of 1–3 (Fig. 3).

UV–vis absorption and fluorescence spectra (Table 2) of the Y-shaped imidazole derivatives reveal that in apolar solvents, the main absorption band is centered around 300 nm, whereas the fluorescence spectrum is centered around 370 nm. The fluorescence spectrum of the imidazole derivative 3 is shifted to lower energies with respect to parent compound 1 in common solvents. These spectral shifts are attributed to the higher inductive electron-acceptor character of the fluorine atom located at C(13) carbon atom. In the case of alcoholic solvents, bathochromic shifts were observed for both absorption and emission providing large Stokes shift. These results suggest an important geometrical rearrangement in the $S_1$ excited state and these observations are in good agreement with the literature report [30].

The higher bathochromic shifts were observed in the fluorescence band of the imidazole derivative 3 with respect to the parent 1 can be interpreted by the Brunings-Corwin effect (Twisted geometry of the imidazole derivative lead the observed bathochromic shift) [31]. The distortion of the geometry in the excited state implies a decrease in the resonance energy, the fluorescence band is bathochromically shifted to a higher extent than the absorption band. Moreover, the loss of planarity in the excited state of the imidazole derivative could explain the lower fluorescence quantum yield in apolar solvents owing to an increase in the non-radiative processes. Taking into account the resonance structures of the imidazole chromophore, we observed that the resonance structure "b" has the largest charge separation along the short molecule axis. Consequently, its contribution would be more important in the $S_0$ ground states than in the $S_1$ excited states. Thus, the polar solvents would stabilize the $S_0$ state more extensively than the $S_1$ state,

**Table 2** Photo physical data of imidazole derivatives 1–3

| Solvents | 1 | | | 2 | | | 3 | | |
|---|---|---|---|---|---|---|---|---|---|
| | $\lambda_{max}$ (nm) | $\lambda_f$ (nm) | $\upsilon_{ss}$ ($cm^{-1}$) | $\lambda_{max}$ (nm) | $\lambda_f$ (nm) | $\upsilon_{ss}$ ($cm^{-1}$) | $\lambda_{max}$ (nm) | $\lambda_f$ (nm) | $\upsilon_{ss}$ ($cm^{-1}$) |
| Hexane | 310.0 | 368.0 | 5084 | 351.0 | 405.0 | 3798 | 360.0 | 410.0 | 3387 |
| Benzene | 309.0 | 368.0 | 5188 | 348.0 | 406.0 | 4105 | 362.0 | 409.0 | 3174 |
| 1,4-Dioxane | 305.7 | 372.0 | 5830 | 350.0 | 409.0 | 4121 | 369.0 | 420.0 | 3290 |
| Diethyl ether | 308.0 | 385.0 | 6493 | 348.0 | 414.0 | 4581 | 370.0 | 425.0 | 3497 |
| Chloroform | 309.0 | 369.0 | 5262 | 350.0 | 408.0 | 4061 | 362.0 | 411.0 | 3293 |
| Ethyl acetate | 306.0 | 380.0 | 6363 | 348.0 | 413.0 | 4522 | 368.0 | 422.0 | 3477 |
| Dichloromethane | 308.0 | 369.0 | 5367 | 348.0 | 408.0 | 4225 | 363.0 | 411.0 | 3217 |
| 1-propanol | 295.0 | 366.0 | 6575 | 344.0 | 418.0 | 5146 | 370.0 | 428.0 | 3662 |
| Ethanol | 297.0 | 377.0 | 7144. | 344.0 | 417.0 | 5088 | 368.4 | 423.0 | 3503 |
| Methanol | 303.0 | 379.0 | 6618 | 344.7 | 413.5 | 4826 | 368.0 | 424.0 | 3589 |
| Acetonitrile | 305.0 | 376.0 | 6191 | 349.0 | 407.0 | 4083 | 371.0 | 423.0 | 3313 |
| DMSO | 304.0 | 379.0 | 6509 | 344.5 | 415.0 | 4931 | 368.5 | 429.0 | 3827 |

thereby increasing the energy gap between both states and explaining the solvatochromic shifts [30].

To analyze the solvatochromic effects, we checked several methods [32–34]. Neither the absorption nor the fluorescence wavenumbers linearly correlate with the Lippert parameter $\Delta f(,n^2)$ [35], which considers the solvent polarity/polarizability or with the Reichardt parameter $E_T^N(30)$ [33, 36], which takes into account several solvent properties (polarity and H-bond donor capacity) in a common parameter. For these reasons, a multi-parameter correlation analysis is employed in which a physicochemical property is linearly correlated with several solvent parameters by means of Eq. 1:

$$(XYZ) = (XYZ)_0 + C_aA + C_bB + C_cC + \ldots \quad (1)$$

where $(XYZ)_0$ is the physicochemical property in an inert solvent and $C_a$, $C_b$, $C_c$ and so forth are the adjusted coefficients that reflect the dependence of the physicochemical property (XYZ) on several solvent properties. Solvent properties that mainly affect the photophysical properties of aromatic compounds are polarity, H-bond donor capacity and electron donor ability. Different scales for such parameters can be found in the literature, Taft et al. [37] propose the $\pi^*$ (dipolarity/polarizability), $\alpha$ (acidity ) and $\beta$ (basicity) scales, whereas more recently Catalan et al. [38] suggest the $SPP^N$, SA and SB scales to describe the polarity/polarizability, the acidity and basicity of the solvents respectively.

Figure 4 shows the obtained correlation between the absorption and fluorescence wavenumbers calculated by the

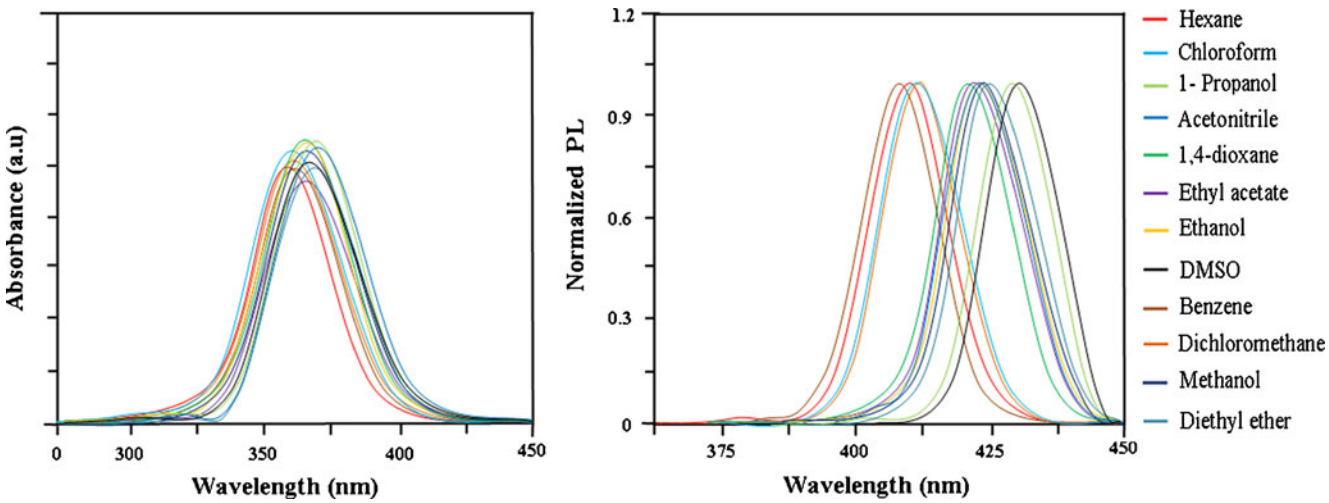


**Fig. 2** Absorption and fluorescence spectra of 3 in various solvents

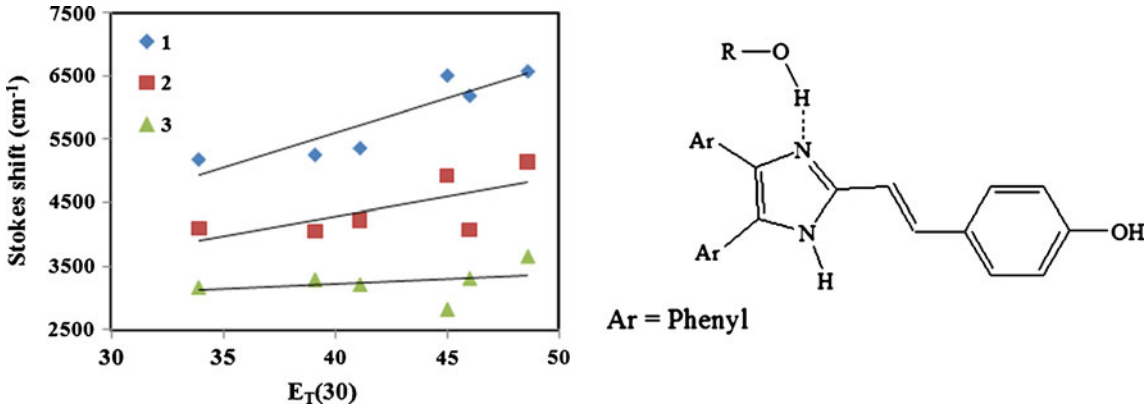


**Fig. 3** Solvation of imidazole derivative and Lippert mataga plot of 1–3

multi-component linear regression employing the Taft-proposed solvent parameters and the experimental values listed in Table 3. Table 3 lists the obtained adjustment and correlation coefficients by the Taft and Catalan parameters. The dominant coefficient affecting the absorption and fluorescence bands of Y-shaped imidazole derivatives 1–3 is that describing the polarity/polarizability of the solvent, $C_{\pi*}$ or $C_{SPP}{}^{N}$ having a positive value, corroborating the above-mentioned solvatochromic shifts with the solvent polarity. The coefficient controlling the H-donor capacity or acidity of the solvent, $C_{\alpha}$ or $C_{SA}$, is the lowest coefficient (Table 3), therefore, the solvent acidity does not play an important role in absorption and fluorescence displacements. The adjusted coefficient representing the electron releasing ability or basicity of the solvent, $C_{\beta}$ or $C_{SB}$ has a negative value, suggesting that the absorption and fluorescence bands shift to lower energies with the increasing electron-donating ability of the solvent. This effect can be interpreted in terms of the stabilization of the resonance structures of the chromophore (Fig. 5). Resonance structure "b" has the positive charge located at the nitrogen atom and it will be stabilized in basic solvents because this resonance structure is predominant in the $S_1$ state, as discussed above and

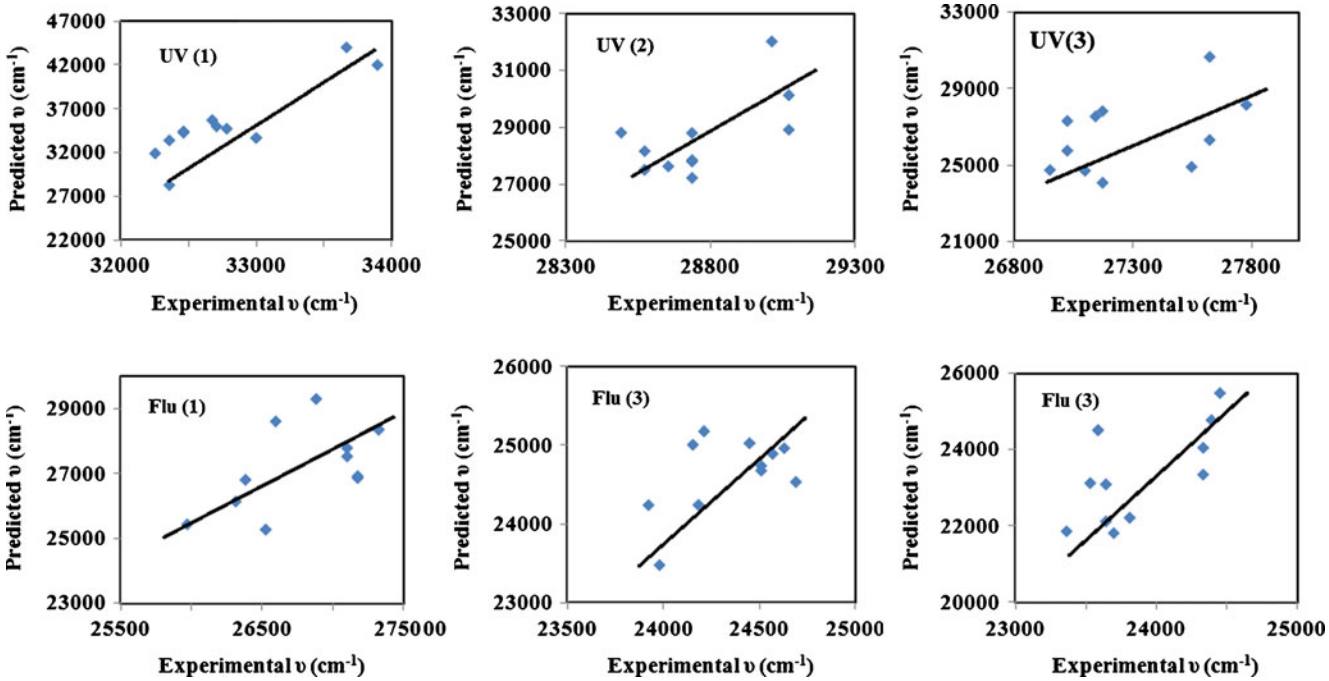


**Fig. 4** Correlation between the experimental absorption and fluorescence wavenumber with the predicted values obtained by a multicomponent linear regression using the π*, α and β-scale (Taft) solvent parameters for 1–3

**Table 3** Adjusted Coefficients ($(\upsilon_x)_0$, $c_a$, $c_b$ and $c_c$) and Correlation Coefficients (r) for the Multilinear Regression Analysis of the Absorption $\upsilon_{ab}$ and Fluorescence $\upsilon_{fl}$ Wavenumbers and Stokes Shift ($\Delta\upsilon_{ss}$) of imidazole derivatives 1–3 with the Solvent Polarity/Polarizability, and the Acid and Base Capacity Using the Taft ($\pi^*$, $\alpha$ and $\beta$) and the Catalan ($SPP^N$, SA and SB) Scales

| | Kamlet-Taft | $(\upsilon_x)_0 cm^{-1}$ | ($\pi^*$) | $c_\alpha$ | $c_\beta$ | r |
|---|---|---|---|---|---|---|
| 1 | $\lambda_{ab}$ | $(3.23\pm0.01)\times10^4$ | $(3.78\pm2.17)\times10^3$ | $-(12.03\pm7.24)\times10^3$ | $(11.41\pm5.82)\times10^3$ | 0.87 |
| | $\lambda_{fl}$ | $(2.71\pm0.01)\times10^4$ | $(2.40\pm2.05)\times10^3$ | $-(16.87\pm7.85)\times10^3$ | $(16.68\pm5.50)\times10^3$ | 0.84 |
| | $\Delta\upsilon_{ss}=\upsilon_{ab}-\upsilon_{fl}$ | $(0.52\pm0.01)\times10^4$ | $(1.38\pm2.31)\times10^3$ | $(4.84\pm7.73)\times10^3$ | $-(5.27\pm6.21)\times10^3$ | 0.91 |
| | Catalan | $(\upsilon_x)_0 cm^{-1}$ | $c_{SPP}{}^N$ | $c_{SA}$ | $c_{SB}$ | r |
| | $\lambda_{ab}$ | $(3.25\pm0.01)\times10^4$ | $(0.22\pm6.66)\times10^3$ | $(20.33\pm17.15)\times10^3$ | $-(31.72\pm17.62)\times10^3$ | 0.90 |
| | $\lambda_{fl}$ | $(2.67\pm0.02)\times10^4$ | $(7.94\pm9.44)\times10^3$ | $-(27.87\pm39.16)\times10^3$ | $(22.95\pm40.21)\times10^3$ | 0.79 |
| | $\Delta\upsilon_{ss}=\upsilon_{ab}-\upsilon_{fl}$ | $(0.58\pm0.03)\times10^4$ | $-(7.71\pm11.39)\times10^3$ | $(48.18\pm47.21)\times10^3$ | $-(54.66\pm48.51)\times10^3$ | 0.54 |
| | Kamlet-Taft | $(\upsilon_x)_0 cm^{-1}$ | ($\pi^*$) | $c_\alpha$ | $c_\beta$ | r |
| 2 | $\lambda_{ab}$ | $(2.86\pm0.00)\times10^4$ | $-(1.66\pm0.88)\times10^3$ | $(6.08\pm2.94)\times10^3$ | $-(4.16\pm2.36)\times10^3$ | 0.87 |
| | $\lambda_{fl}$ | $(2.46\pm0.00)\times10^4$ | $(0.54\pm1.01)\times10^3$ | $-(3.81\pm3.37)\times10^3$ | $(2.75\pm2.71)\times10^3$ | 0.90 |
| | $\Delta\upsilon_{ss}=\upsilon_{ab}-\upsilon_{fl}$ | $(0.40\pm0.00)\times10^4$ | $-(2.20\pm0.46)\times10^3$ | $(9.89\pm4.61)\times10^3$ | $-(6.90\pm3.70)\times10^3$ | 0.93 |
| | Catalan | $(\upsilon_x)_0 cm^{-1}$ | $c_{SPP}{}^N$ | $c_{SA}$ | $c_{SB}$ | r |
| | $\lambda_{ab}$ | $(2.87\pm0.00)\times10^4$ | $-(0.46\pm1.97)\times10^3$ | $(7.90\pm8.18)\times10^3$ | $-(10.15\pm8.40)\times10^3$ | 0.84 |
| | $\lambda_{fl}$ | $(2.44\pm0.01)\times10^4$ | $(2.93\pm3.71)\times10^3$ | $-(20.06\pm15.40)\times10^3$ | $(23.94\pm15.81)\times10^3$ | 0.66 |
| | $\Delta\upsilon_{ss}=\upsilon_{ab}-\upsilon_{fl}$ | $(0.42\pm0.01)\times10^4$ | $-(3.39\pm5.06)\times10^3$ | $(27.97\pm20.96)\times10^3$ | $-(34.10\pm21.53)\times10^3$ | 0.78 |
| | Kamlet-Taft | $(\upsilon_x)_0 cm^{-1}$ | ($\pi^*$) | $c_\alpha$ | $c_\beta$ | r |
| 3 | $\lambda_{ab}$ | $(2.76\pm0.00)\times10^4$ | $-(4.66\pm0.80)\times10^3$ | $(10.95\pm2.62)\times10^3$ | $-(7.45\pm2.15)\times10^3$ | 0.94 |
| | $\lambda_{fl}$ | $(2.47\pm0.00)\times10^4$ | $-(3.58\pm1.15)\times10^3$ | $(6.03\pm3.86)\times10^3$ | $-(3.77\pm3.10)\times10^3$ | 0.95 |
| | $\Delta\upsilon_{ss}=\upsilon_{ab}-\upsilon_{fl}$ | $(0.42\pm0.01)\times10^4$ | $-(1.08\pm1.04)\times10^3$ | $(4.92\pm3.49)\times10^3$ | $-(3.68\pm2.80)\times10^3$ | 0.79 |
| | Catalan | $(\upsilon_x)_0 cm^{-1}$ | $c_{SPP}{}^N$ | $c_{SA}$ | $c_{SB}$ | r |
| | $\lambda_{ab}$ | $(2.73\pm0.01)\times10^4$ | $(1.53\pm6.47)\times10^3$ | $-(10.29\pm26.82)\times10^3$ | $(12.06\pm27.54)\times10^3$ | 0.75 |
| | $\lambda_{fl}$ | $(2.40\pm0.01)\times10^4$ | $(3.74\pm7.82)\times10^3$ | $-(22.68\pm32.43)\times10^3$ | $(25.46\pm33.31)\times10^3$ | 0.34 |
| | $\Delta\upsilon_{ss}=\upsilon_{ab}-\upsilon_{fl}$ | $(0.34\pm0.00)\times10^4$ | $-(2.21\pm2.38)\times10^3$ | $(12.39\pm9.85)\times10^3$ | $-(13.40\pm10.12)\times10^3$ | 0.60 |

the stabilization of the $S_1$ state with the solvent basicity would be more important than that of the $S_0$ state. Consequently, the energy gap between the $S_1$ and $S_0$ states decreases and the absorption and fluorescence wavelengths shift to longer wavelengths with increasing solvent basicity.

## Conclusions

The presence of cinnamaldehyde ring at C(2) in the Y-shaped imidazole chromophore core originates a distortion from planarity in the imidazole units, mainly in the excited state, which leads to an increase in the rate constant of non-radiative deactivation and in the stokes shift. Both photophysical factors have an opposite effect on the lasing efficiency. Thus, the increase in the loss of the resonator cavity due to the augmentation in the non-radiative processes could be compensated to some extent by a reduction in the reabsorption and reemission losses, owing to the higher stokes shift. From this photophysical studies, polar solvents are recommended to obtain the highest optical efficiencies in liquid media.

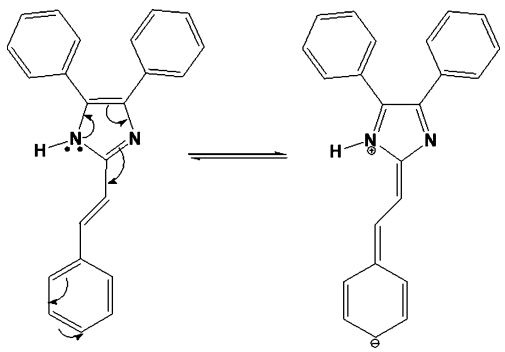


**Fig. 5** Resonance structures of the imidazole chromophore (3)

**Acknowledgements** One of the author Dr. J. Jayabharathi, Associate Professor in Chemistry, Annamalai University is thankful to Department of Science and Technology [No. SR/S1/IC-07/2007], University Grants commission (F. No. 36-21/2008 (SR)) for providing fund to this research work.

## References

1. Santos J, Mintz EA, Zehnder O, Bosshard C, Bu XR, Gunter P (2001) New class of imidazoles incorporated with thiophenevinyl conjugation pathway for robust nonlinear optical chromophores. Tetrahedron Lett 42:805–808
2. Hung WS, Lin JT, Chien CH, Tao YT, Sun SS, Wen YS (2004) Highly phosphorescent bis-cyclometallated iridium complexes containing benzoimidazole-based ligands. Chem Mater 16:2480–2488
3. Chen CH, Shi J (1998) Metal chelates as emitting materials for organic electroluminescence. Coord Chem Rev 171:161–174
4. Kamidate T, Yamaguchi K, Segawa T (1989) Lophine chemiluminescence for determination of chromium (VI) by continuous flow method. Anal Sci 5:429–433
5. MacDonald A, Chain KW, Nieman TA (1979) Lophine chemiluminescence for metal ion determinations. Anal Chem 51:2077–2082
6. Marino DF, Ingle JD Jr (1981) Determination of chromium (VI) in water by lophine chemiluminescence. Anal Chem 53:294–298
7. Chou PT, McMorrow D, Aartsma TJ, Kasha M (1984) The proton-transfer laser. Gain spectrum and amplification of spontaneous emission of 3-hydroxyflavone. J Phys Chem 88:4596–4599
8. Keck J, Roessler M, Schroeder C, Stueber GJ, Waiblinger F, Stein M, Legourrierec D, Kramer HEA, Hoier H, Henkel S, Fischer P, Port H, Hirsch T, Tytz G, Hayoz P (1998) Ultraviolet absorbers of the 2-(2-Hydroxyaryl)-1,3,5-triazine class and their methoxy derivatives: fluorescence spectroscopy and x-ray structure analysis. J Phys Chem A 102:6975–6985
9. Martinej ML, Cooper WC, Chou PT (1992) A novel excited-state intramolecular proton transfer molecule, 10-hydroxybenzo[h] quinoline. Chem Phys Lett 193:151–154
10. Wu Y, Peng X, Fan J, Gao S, Tian M, Zhao J, Sun S (2007) Fluorescence sensing of anions based on inhibition of excited-state intramolecular proton transfer. J Org Chem 72:62–70
11. Shah M, Thangaraj K, Soong ML, Wolford LT, Boyer JH, Politzer IR, Pavlopoulos TG (1990) Pyrromethene-BF2 complexes as laser dyes. Part 1. Heteroat Chem 1:389–399
12. Paviopoulos TG, Boyer JH, Thangaraj K, Sathyamoorthi G, Shah MP, Soong ML (1992) Laser dye spectroscopy of some pyrromethene-$BF_2$ complexes. Appl Opt 31:7089–7094
13. Costela A, Garcia-Moreno I, Gomez C, Sastre R, Amat-Guerri F, Liras M, Lopez Arbeloa F, Banuelos Prieto J, Lopez Arbeloa I (2002) Photophysical and lasing properties of new analogs of the boron−dipyrromethene laser dye PM567 in liquid solution. J Phys Chem A 106:7736–7342
14. Guassian 03 program, (Gaussian Inc., Wallingford CT) 2004
15. Jayabharathi J, Thanikachalam V, Saravanan K, Srinivasan N (2010) Iridium(III) complexes with orthometalated imidazole ligands subtle turning of emission to the saturated green colour. J Fluoresc. doi:10.1007/s10895- 010-0737-7
16. Saravanan K, Srinivasan N, Thanikachalam V, Jayabharathi J (2010) Synthesis and photophysics of some novel imidazole derivatives used as sensitive fluorescent chemisensors. J Fluoresc 21:65–80
17. Gayathri P, Jayabharathi J, Srinivasan N, Thiruvalluvar A, Butcher RJ (2010) 2-(4-Fluorophenyl)-4,5-dimethyl-1-(4-methylphenyl)-1H-imidazole. Acta Crystallogr E 66:o1703
18. Jayabharathi J, Thanikachalam V, Venkatesh Perumal M, Saravanan K (2011) Displacement reaction using ibuprofen in a mixture of bioactive imidazole derivative and bovine serum albumin–a fluorescence quenching study. J Fluoresc. doi:10.1007/s10895-011-0878-3
19. Jayabharathi J, Thanikachalam V, Venkatesh Perumal M, Srinivasan N (2011) Fluorescence resonance energy transfer from a bio-active imidazole derivative 2-(1-phenyl-1H-imidazo[4,5-f][1,10]phenanthrolin-2-yl)phenol to a bioactive indoloquino lizine system. Spectrochim Acta A 79:236–244
20. Jayabharathi J, Thanikachalam V, Saravanan K, Srinivasan N, Venkatesh Perumal M (2010) Physiochemical properties of organic nonlinear optical crystal from a combined experimental and theoretical study. Spectrochim Acta A 78:794–802
21. Jayabharathi J, Thanikachalam V, Jayamoorthy K, Venkatesh Perumal M (2011) Physiochemical studies of excited state intramolecular proton transfer process Luminescent chemosensor by spectroscopic investigation supported by ab initio calculations. Spectrochim Acta A 79:6–16
22. Gayathri P, Jayabharathi J, Srinivasan N, Thiruvalluvar A, Butcher RJ (2010) 4,5-Dimethyl-2-phenyl-1-(*p*-tolyl)-1*H*-imidazole. Acta Crystallogr E 66:o2826
23. Jayabharathi J, Thanikachalam V, Saravanan K (2009) Effect of substituents on the photoluminescence performance of Ir(III) complexes: synthesis, electrochemistry and photophysical properties. J Photochem Photobiol A Chem 208:13–20
24. Jayabharathi J, Thanikachalam V, Srinivasan N, Saravanan K (2010) Synthesis, structure, luminescent and intramolecular proton transfer in some imidazole derivatives. J Fluoresc. doi:10.1007/s10895-010-0747-5
25. Jayabharathi J, Thanikachalam V, Venkatesh Perumal M (2011) Mechanistic investigation on binding interaction of bioactive imidazole with protein bovine serum albumin - A biophysical study. Spectrochim Acta Part A 79:502–507. doi:dx.doi.org
26. Jayabharathi J, Thanikachalam V, Saravanan K, Venkatesh Perumal M (2011) Spectrofluorometric studies on the binding interaction of bioactive imidazole with bovine serum albumin: a DFT based ESIPT process. Spectrochim Acta A 79:1240–1246
27. Flom SR, Barbara PF (1983) (1983), The photodynamics of 2-(2′-hydroxy-5′-methylphenyl)-benzotriazole in low-temperature organic glasses. Chem Phy Lett 94:488–493
28. Balamurali MM, Dogra SK (2004) Intra- and intermolecular proton transfer in methyl-2-hydroxynicotinate. J Luminescence 110:147–163
29. Mazumdar S, Manoharan R, Dogra SK (1989) Solvatochromic effects in the fluorescence of a few diamino aromatic compounds. J Photochem Photobiol A 46:301–314
30. Bergstrom F, Mikhalyov I, Hagglof P, Wortmann R, Ny T (2002) Dimers of dipyrrometheneboron difluoride (BODIPY) with light spectroscopic applications in chemistry and biology. J Am Chem Soc 124:196–204
31. Hofer JE, Grabenstetter RJ, Wiig EO (1950) The fluorescence of cyanine and related dyes in the Monomeric State. J Am Chem Soc 72:203–209
32. Marcus Y (1993) The properties of organic liquids that are relevant to their use as solvating solvents. Chem Soc Rev 22:409–416
33. Reichardt C (1994) Solvatochromic dyes as solvent polarity indicators. Chem Rev 94:2319–2358

34. Catalan J (1997) On the E(T) (30), pi, P(y), S', and SPP empirical scales as descriptors of nonspecific solvent effects. J Org Chem 62:8231–8234
35. Lippert E (1975) Organic molecular photophysics. In: Birks JB (ed) Wiley-Interscience, Bristol
36. Dimroth K, Reichardt C (1969) Of pyridinium *N-phenol* betaines and their use for characterizing the polarity of solvents, V expansion of the solvent polarity scale by using alkyl-substituted pyridinium *N-phenol* betaines. Liebigs Ann Chem 727:93–105
37. Kamlet MJ, Taft RW (1976) The solvatochromic comparison method. I. The $\beta$-scale of solvent hydrogen-bond acceptor (HBA) basicities. J Am Chem Soc 98:377–383
38. Catalan J, Lopez V, Perez P (1996) Use of the SPP scale for the analysis of molecular systems with dual emissions resulting from the solvent polarity. J Fluoresc 6:15–22